metals

MDPI

Article

Comparative Study of Jet Slurry Erosion of Martensitic Stainless Steel with Tungsten Carbide HVOF Coating

Galileo Santacruz [1,*], Antonio Shigueaki Takimi [1], Felipe Vannucchi de Camargo [1,2], Carlos Pérez Bergmann [1] and Cristiano Fragassa [2]

[1] Post-Graduation Program in Mining, Metallurgical and Materials Engineering, Federal University of Rio Grande do Sul, Av. Osvaldo Aranha 99, Porto Alegre 90035-190, Brazil; antonio.takimi@gmail.com (A.S.T.); felipe.vannucchi@unibo.it (F.V.d.C.); bergmann@ufrgs.br (C.P.B.)

[2] Department of Industrial Engineering, University of Bologna, Viale del Risorgimento 2, 40136 Bologna, Italy; cristiano.fragassa@unibo.it

* Correspondence: galileo.santacruz@ufrgs.br; Tel.: +55-(51)-3308-3637

Received: 30 April 2019; Accepted: 17 May 2019; Published: 24 May 2019

Abstract: This work evaluates the behavior of a martensitic stainless steel (AISI 410) thermally treated by quenching and tempering with a tungsten carbide (86WC-10Co-4Cr) coating obtained by high-velocity oxygen fuel (HVOF) thermal spray deposition, analyzing the volume loss under erosive attacks at 30° and 90° incidence angles by using jet slurry erosion equipment with electrofused alumina erodent particles. Firstly, the characterization of the samples was carried out in terms of the microstructure (SEM), thickness, roughness, porosity, and microhardness. Then, samples were structurally characterized in the identification of the phases (XRD and EDS) present in the coating, as well as the particle size distribution (LG) and morphology of the erodent. It was determined that the tungsten carbide coating presented better resistance to jet slurry erosion wear when compared to the martensitic stainless steel analyzed, which is approximately two times higher for the 30° angle. The more ductile and brittle natures of the substrate and the coating, respectively, were evidenced by their higher volumetric erosion at 30° for the first and 90° for the latter, as well as their particular material removal mechanisms. The enhanced resistance of the coating is mainly attributed to its low porosity and high WC-Co content, resulting in elevated mechanical resistance.

Keywords: tribology; wear; slurry erosion; coating; cermet

1. Introduction

The erosion of metallic materials due to slurry erosion is a recurrent and common problem in various industrial applications, such as hydraulic turbines for hydroelectric plants and mud pumps, as well as the processing of minerals and pipes for the petrochemical industry. The effect caused by the particulate material in the liquid represents a major industrial problem, affecting the life of components, reducing their performance, and demanding continuous preventive and corrective maintenance, bearing elevated financial and environmental costs to the supply chain of products as a whole. Thus, when designing parts that will be subjected to erosive wear, the proper choice of engineering materials plays a key role in decreasing this wear rate, and assures adequate tribological behavior [1].

Supported by recent research, the technology of surface treatments and coatings of thin films have been demonstrated to be a valid and efficient way to improve the resistance of metallic-coated materials [2], whereas understanding and studying the surface wear mechanisms is vital to predicting

failures by erosion and corrosion, providing adequate dimensioning of parts and relying on optimized properties aggregated by the coatings.

Among the coated materials, some of the most relevant ones are martensitic stainless steels, given their wide range of industrial applications. These are commonly adopted for regular ends, such as in the automotive industry [3], but may also be used in the cutting-edge design of complex structures, such as nuclear reactors [4] and power plants [5]. Martensitic stainless steels are high-carbon-content alloys (0.1–1.2%) with chromium (12–18%), presenting magnetic properties, elevated strength, low-temperature toughness, and good corrosion resistance [6], as well as better mechanical resistance to erosive particles than austenitic steel [7].

Cermet materials have shown excellent resistance to erosive wear, increasing the resistance, for instance, of hydro-turbine parts [8], being able to noticeably improve the resistance of originally uncoated metallic pieces to erosion, corrosion, or both, especially at high temperatures [9]. Kumar et al. [8] demonstrated the enhanced abrasive wear resistance properties provided by WC-Co, which can have their corrosion resistance increased with the addition of a small amount of Cr. For this reason, the composition of WC-10% Co-4% Cr is widely considered in coatings for applications in components of hydric companies to prolong their operational life [8]. Coatings of WCCoCr are usually deposited with a High-Velocity Oxy-Fuel (HVOF) thermal spray process [10].

HVOF has demonstrated to be highly effective in the obtention of low-porosity adherent coatings [11–13], whereas the mechanical properties of the coated material are shielded by coatings with high compressive and tensile strengths and elevated hardness. Furthermore, as demonstrated by Liu et al. [14] and Hou et al. [15], HVOF coatings can enhance the resistance of parts against cavitation erosion–corrosion due to its features of high flame velocity, low flame temperature, and the possibility of producing dense coatings with less decarburization and low oxide content.

These coatings are mainly prepared with WC-based cermets, once the alliance of the hard WC phase with a ductile metal in different proportions can produce materials with a significantly wide range of properties [16]. This metallic phase is usually cobalt or nickel, the latter contributing to the enhancement of the material's corrosion resistance. In general, the high hardness and fracture toughness of WC cermets make them suitable materials to improve abrasion resistance in many industrial applications, such as hydraulic machinery and coastal installations [17].

The present investigation evaluates the erosive wear of the coating 86WC-10% Co-4% Cr when deposited by HVOF using feedstock materials on quenched and tempered martensitic stainless steel (AISI 410), and how it upgrades its original erosion resistance. The volume loss under jet slurry erosion for incidence angles of 30° and 90° between the axis of symmetry of the fluid flow and the surface of the samples was evaluated, including controlling parameters such as the angle and speed of impact, test temperature, and concentration of erosive particles in the suspension. Electrofused alumina was used as erodent material. The materials were characterized with regard to their microstructure by scanning electron microscopy (SEM), light microscopy (LM), thickness, roughness, porosity, microhardness, and phase structure by X-ray diffraction (XRD) and energy dispersive spectroscopy (EDS). Also, the particle size distribution was analyzed by laser granulometry (LG), and the morphology of the erodent was identified.

2. Materials and Methods

2.1. Substrate Material

Martensitic stainless steel (AISI 410) cylinders which were 30 mm in diameter and 10 mm in height were used [18]. The steel samples were austenitized at 1263 K for 35 min, then oil-quenched and tempered at 793 K for 35 min afterward. The microstructure obtained after this procedure was composed of martensite with some precipitated carbides on the grain contours, a typical outcome of quenching and tempering thermal treatments [6] (Figure 1).

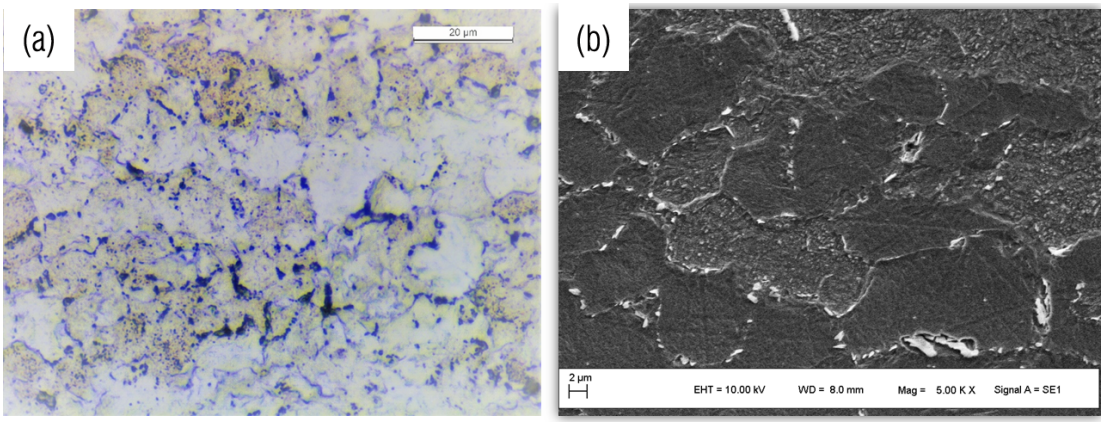

Figure 1. Resulting microstructure of AISI 410 stainless steel after thermal treatments by (**a**) LM 1000×, and (**b**) SEM 5000×, after Vilella acid etching.

2.2. HVOF Coating

Spherical fine powders WOKA-3653 (86WC-10Co-4Cr) from Oerlikon Metco (Pfaffikon, Switzerland) were used with a particle size distribution of nominal range $-45 + 11$ µm and apparent density 4.8–5.8 g/cm^3 [19]. The approximate chemical composition of the WOKA-3653 powder is given in Table 1. HVOF spraying parameters are briefly listed in Table 2.

Table 1. Chemical composition of WOKA-3653 (wt %) [19].

Elements	Composition (%)
W	Balance
Co	8.5–11.5
Cr	3.4–4.6
C (Total)	4.8–5.6
Fe (Max)	0.2

Table 2. Coating parameters of high-velocity oxygen fuel (HVOF) equipment.

Spray Parameters	Value
*P*ropylene flow rate	4620 (L/h)
*O*xygen flow rate	15,180 (L/h)
*P*owder feed rate	42 (g/min)
*S*pray distance	230 (mm)

2.3. Erodent Particles

The particle size distribution of the alumina erodent (Al_2O_3) was measured using the Cilas 1180 laser diffraction particle size analyzer (Cilas Ariane Group, Le Barp, France) according to the ISO 13320:2009 standard [20]. The abrasive particle size distribution is shown in Figure 2, showing results of the average abrasive particle size of approximately 98.55 µm. Furthermore, irregular angular-shaped particles are depicted by the SEM micrograph in Figure 3.

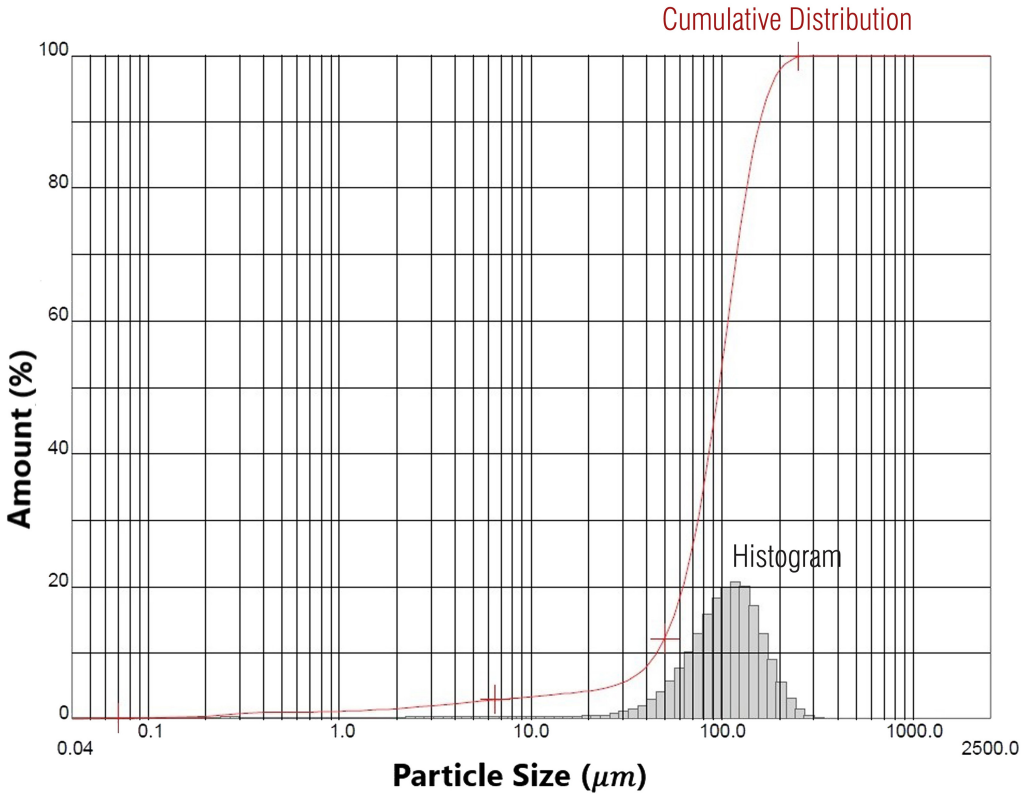

Figure 2. Particle size distribution of aluminium oxide and cumulative distribution.

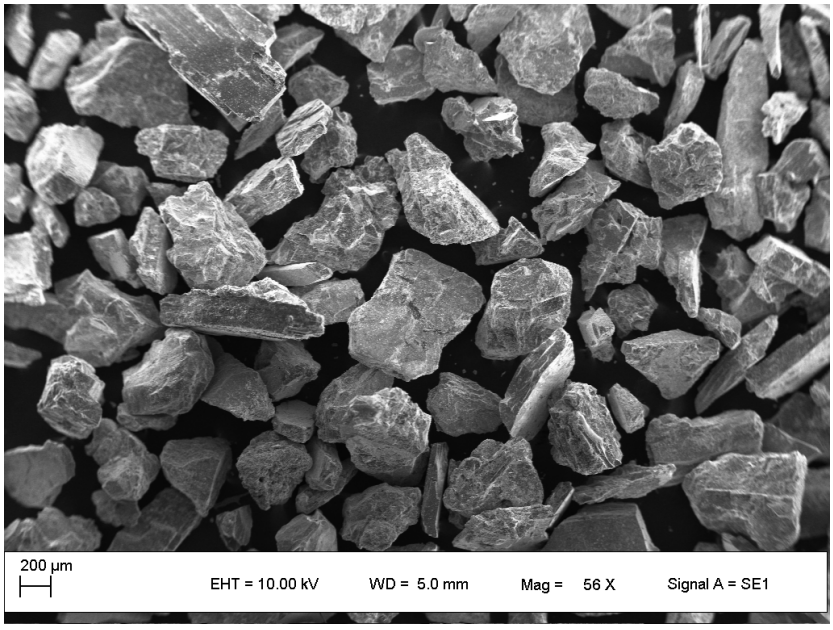

Figure 3. SEM image showing the abrasive particles' shape and size (56×).

2.4. Microstructural and Qualitative Phase Characterization

The microstructure characterization was done in an EVO MA10 SEM (ZEISS, Oberkochen, Germany) and using a light microscope, LEICA DM2700 M. The total porosity of the coatings was measured through digital image analysis following the ASTM E2109-01 standard [21]. The surface roughness of the steel and as-sprayed samples were measured before jet slurry erosion testing, and

after it using a surface roughness tester Mitutoyo SJ-400 (Mitutoyo America Corporation, Aurora, IL, USA). Then, cross-sectional Vickers microhardness measurements were performed using a Buehler Micromet 2001 microhardness tester (HV300 g, 30 s, BUEHLER Ltd., Lake Bluff, IL, USA) according to the ASTM E-384-11 standard [22]. To identify the phases in the coatings and to understand the phase formation during coatings' build-up, surface XRD analysis of the as-sprayed samples was carried out using the PHILIPS Xpert MDP X-ray diffractometer (PHILIPS, Amsterdam, The Netherlands) with Cu-Kα radiation. Lastly, localized compositional analyses of the coated specimens were done with a SHIMADZU SSX-550 EDS spectrometer (SHIMADZU CORPORATION, Nishinokyo Kuwabara-cho, Nakagyo-ku, Kyoto, Japan) coupled to the EVO MA10 SEM.

2.5. Jet Slurry Erosion Tests

The jet slurry erosion tests were carried out in a modified commercial high-pressure washer Electrolux UWS10 (Electrolux Group, Stockholm, Sweden) based on the ASTM G-76 standard [23–27]. A feeding system for the erodent particles was adapted in the nozzle of the gun using an internal Venturi accelerator inside the test chamber. This equipment allows for control over the angle of impact, the speed of impact, the concentration of erodent particles in the suspension, and the test temperature. Figure 4 shows the configuration of the testing advice.

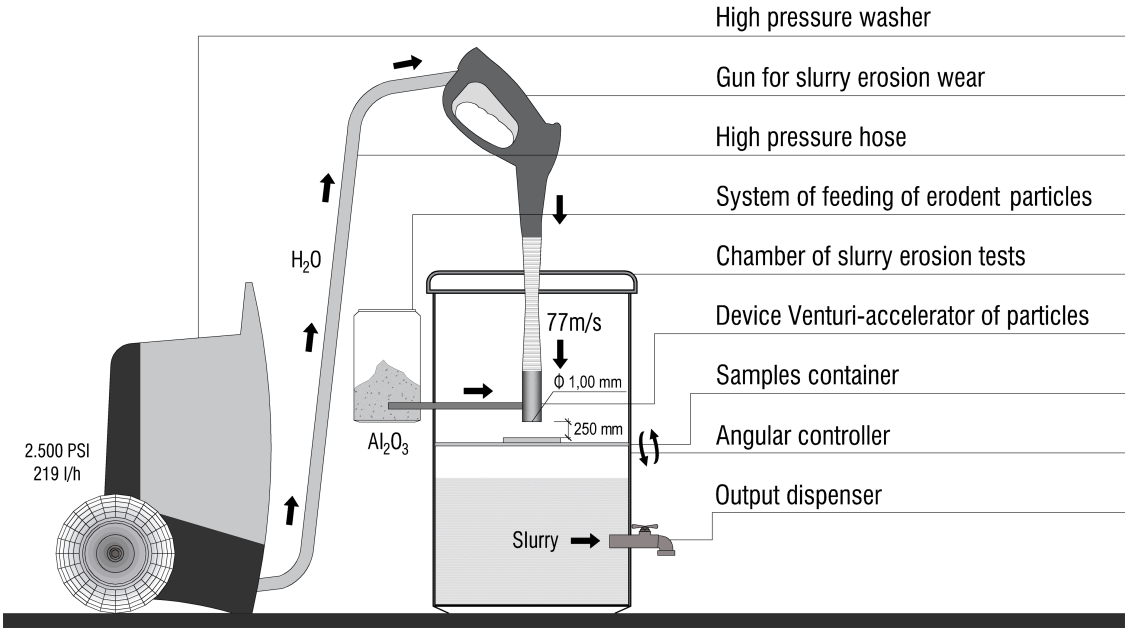

Figure 4. Schematic diagram of the jet slurry erosion tester.

The tests were performed using water between 25 °C and 28 °C with 960 g of erodent. The samples were placed at the nozzle output to guarantee the incidence of impact fluid and mean jet velocity of erosive material in a suspension of 77 m/s. This velocity was calculated using the flow rate, time, and nozzle area measurements of the flow output. The incidence angles studied were 30° and 90° between the axis of symmetry of the fluid flow and the surface of the samples. In all cases, the concentration of particles in the slurry was approximately 7 wt % [28–30]. The erosion resistance was determined from the volume loss results per unit of time, from the difference of the mass loss, considering the relation of the apparent density of the studied materials (adopting substrate as 7.73 g/cm^3 and coating as 12.5 g/cm^3 [31–33]. Mass losses were measured in three samples of coating and three of substrate every 1 min until reaching a total erosion time of 4 min by using a scale with 0.01 mg resolution. The total duration of each test was 4 min. The samples were cleaned in an ultrasonic bath with deionized water before and after each test. Then, after the cleaning operation, they were dried and weighted.

3. Results and Discussion

3.1. X-ray Diffraction Analysis

Figure 5 shows the XRD pattern of the 86WC-10Co-4Cr coating obtained by HVOF with the powder WOKA-3653, where the WC (JCPDS 00-051-0939) and W (JCPDS 01-089-2767) phases can be promptly identified by using the Joint Committee on Powder Diffraction Standards (JCPDS) [34]. The XRD pattern shows that WC is predominant in the powder diffractogram. It is also possible to verify the presence of W and Co as secondary phases formed during the thermal spraying process by the decarburization of WC particles, also reported by other researchers [30,35,36]. The lack of identification of the Co peak by XRD in this figure is justified by the low content of the metal in the coating, and its diffraction peak is most likely situated among the noise range in the graph.

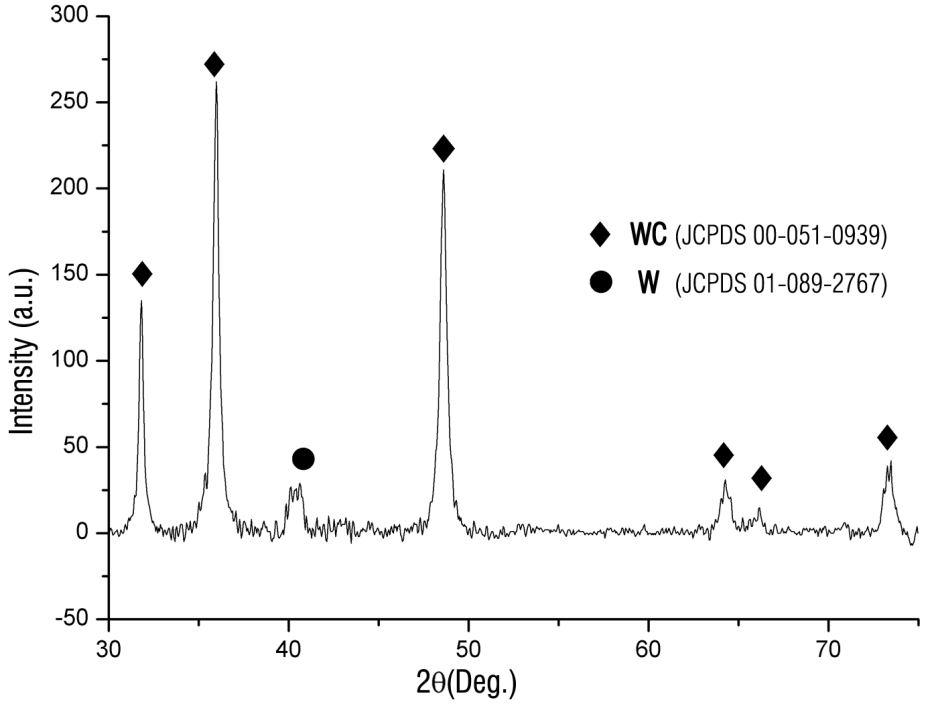

Figure 5. XRD pattern of the HVOF 86WC-10Co-4Cr coating.

3.2. EDS Analysis Coating

Figure 6 shows the elemental microanalysis of one of the regions of the coating cross-section that were scanned using the EDS system, exhibiting the presence of W, Co, Cr, and C in the samples. Figure 7 corroborates the presence of these elements in a quantitative pattern, which agrees with Figure 5, demonstrating a predominance of tungsten. Similar results were found by Thakur et al. [37], considering coatings with the same composition and deposition technique.

3.3. Mechanical Properties of Materials

Figure 8 shows the micrograph of the HVOF 86WC-10Co4Cr coating. It presents a continuous shape and homogeneous microstructure, with a low presence of cracks and pores. It is not possible to distinguish any lamellar structure. This can be explained by a possible melting of the binder metal, which induces a better distribution in the coating material [38]. The average thickness of the HVOF 86WC-10Co-4Cr coating was calculated using micrographs of cross-sections processed using ImageJ software, and among 100 to 200 measurements were performed on different samples for the obtainment of an arithmetic mean of circa 227 μm.

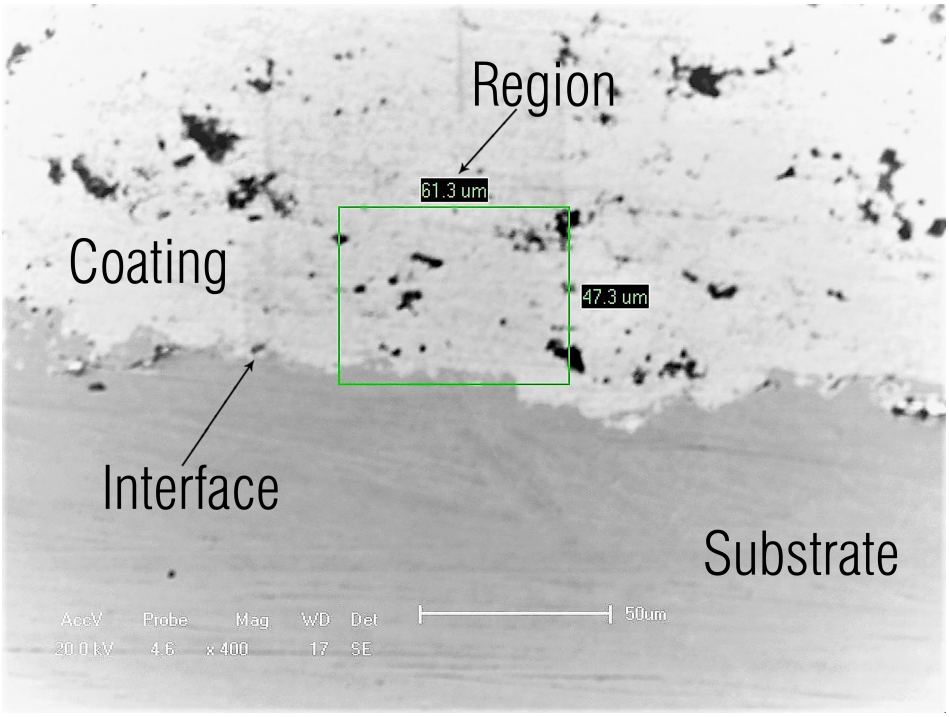

Figure 6. SEM image of the elemental microanalysis region in the cross-section of the HVOF 86WC-10Co4Cr coating using the EDS system (400×).

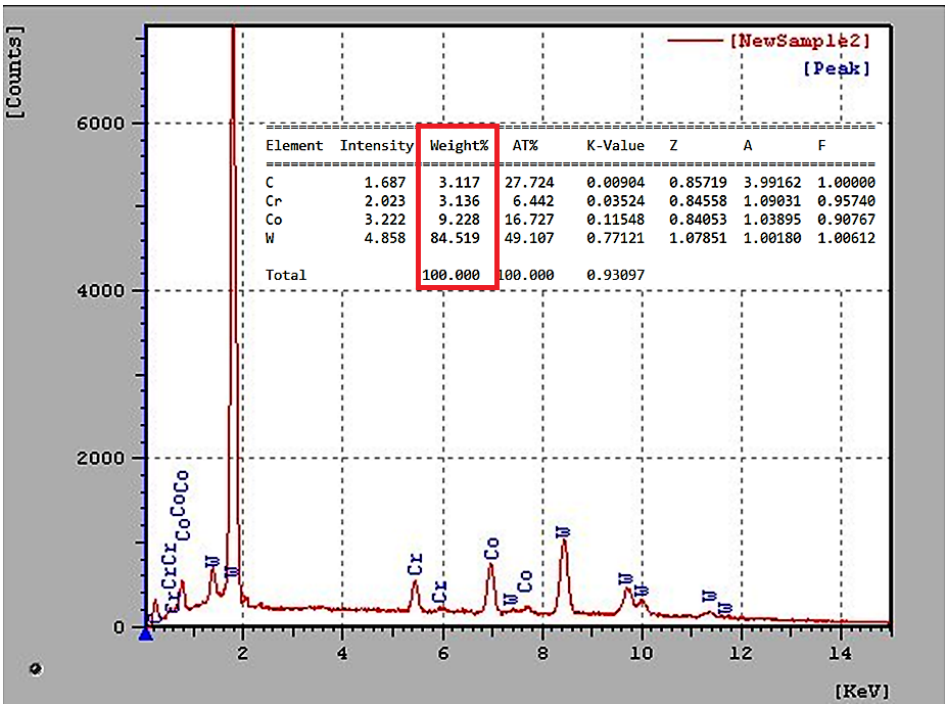

Figure 7. Quantitative pattern of the elemental microanalysis region in the cross-section of the HVOF 86WC-10Co-4Cr coating using the EDS system.

Three analyses of the coating were measured in each one of three samples through digital image analysis according to ASTM E2109-01 [21], yielding an average porosity of 0.7%, which is considered acceptable within the values presented in the literature and according to the criterion specified by the manufacturer Oerlikon Metco of a mean porosity lower than 1.0% [8,10,37].

Microhardness reflects the microstructure and the physical and mechanical properties of both substrate and coating, which in turn are dependent on the materials and processes employed in their manufacture. Hardness is a property that can be considered to be variable throughout the coating in certain zones, due to eventual heterogeneities of the material. For this reason, when measuring this property, one must consider the preparation of the surface, the section analyzed, as well as the number of indentations performed. The microhardness of the coating and substrate are presented in Table 3. The hardness value of the coating is compatible with the literature, and is in agreement with the specification of the coating powder's manufacturer (750 to 1450 HV0.3) [19].

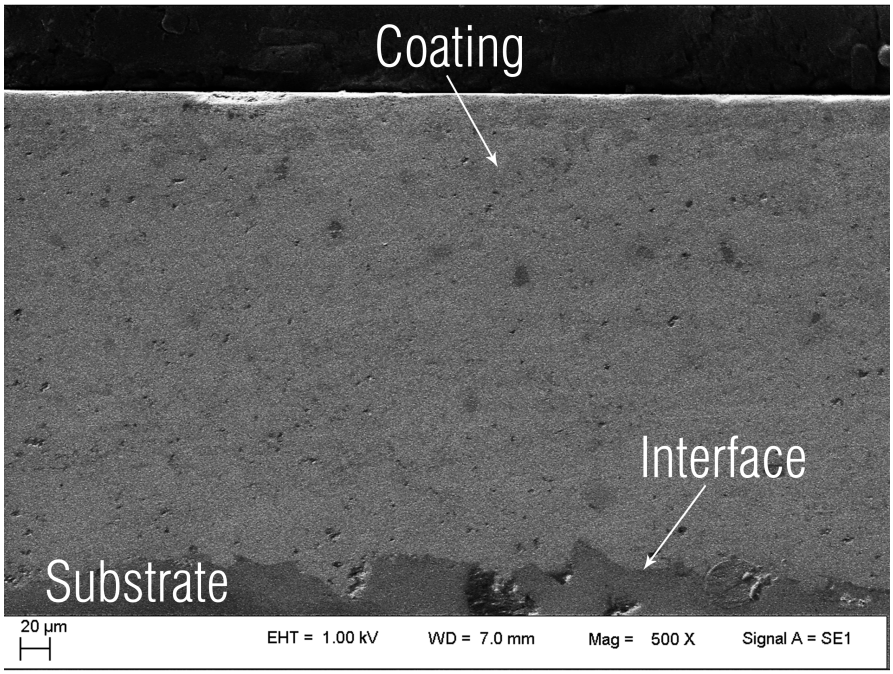

Figure 8. SEM image of the microstructure of the HVOF 86WC-10Co-4Cr coating in the cross-section (500×).

Table 3. Results of Vickers microhardness measurements—cross-section (HV0.3-2.94N).

Material / Coating	86WC-10Co4Cr	Steel AISI 410
Microhardness average	1139	219
Standard Deviation	171	31
Coefficient of Variation (%)	15	14

According to the microhardness values along the cross-section of the spray coating, there were variations due to the distribution of the phases. Castro et al. [39] demonstrated that it is possible to observe this effect when working with sublayers (sprayed coatings), as microhardness values may vary since each indentation point can be placed in different microstructures—in this case, carbides, oxides, inclusions, and the matrix itself.

Trelleborg [40] describes WC-based materials as metal–ceramic composites in which the microhardness values found are associated with each microconstituent. By its turn, the microstructure depends on factors such as the composition of each phase, the morphology of the powder, the spray technique, and the porosity.

The highest value of microhardness performed on the 86WC-10Co-4Cr coating was 1448 HV0.3, being also the closest one to the manufacturer's specification [19]. Thakur et al. [37] and Castro et al. [39] obtained similar results of 1297 ± 45 HV0.3 and 1256 HV, respectively, for WC-CoCr coatings sprayed by HVOF. In the same way, Kumar et al. [8], Maiti et al. [30], Berger et al. [41], and Ahmed et al. [42]

reported microhardness values of 1031 ± 99, 1180 ± 70, 1118 ± 131, and 1106 HV0.3 for similar sprayed coatings applied by the same technique, respectively.

The indentation performed on the substrate, corresponding to thermally treated martensitic stainless steel measured microhardness values, was 219 HV0.3, which is once again very similar to that reported by Maiti et al. [30] of 199 HV0.3.

Table 4 shows the accumulated erosion rate by the mass of erodent in loss of volume of the samples tested as a function of the impact angle for both the substrate and coating in a total time of 4 min.

Table 4. Accumulated erosion rate in volume loss.

Material/Coating	Impact Angle (°)	Volumetric Erosion Rate ($cm^3_{target}/g_{erodent}$) × 10^{-5}	Standard Deviation ($cm^3_{target}/g_{erodent}$) × 10^{-5}
Steel AISI 410	30	0.8449	0.0114
	90	0.7025	0.0495
86WC-10Co4Cr	30	0.4490	0.0023
	90	0.6778	0.0283

Figures 9 and 10 show the mass losses measured in three samples of coating and three of substrate every 1 min until a total erosion time of 4 min was reached for the impact angles of 30° and 90°, respectively. Steel exhibits a much higher level of erosive wear at an impact angle of 30° rather than at 90°, demonstrating ductile behavior with a ploughing-predominant material removal mechanism, as is reported in the literature [43,44]. Furthermore, many authors confirm that metals present an enhanced erosion rate at lower angles [45–48]. Figure 10 also shows that, for the impact angle of 90°, the tungsten carbide coating presented an accumulated volumetric erosion rate that is slightly lower than the martensitic stainless steel.

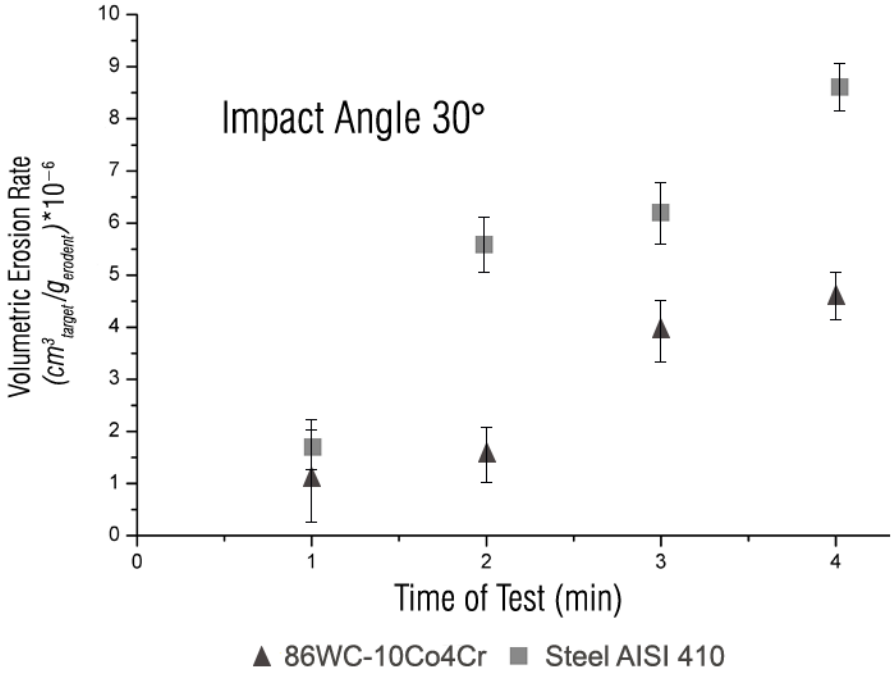

Figure 9. Variation of the accumulated volumetric erosion rate as a function of the impact angle of 30° for the martensitic stainless steel (AISI 410) and tungsten carbide (86WC-10Co-4Cr) coating.

On the other hand, when comparing Figures 9 and 10, it can be seen that the coating presents higher erosive wear at an angle of impact of 90° than at 30°, indicating the coating's fragile behavior. This is due to the repeated action of the erosive perpendicular particles impacted on the surface, producing microfractures that contribute to the wear of the WC hard metal and resulting in its eventual removal, agreeing with the results found in [49,50].

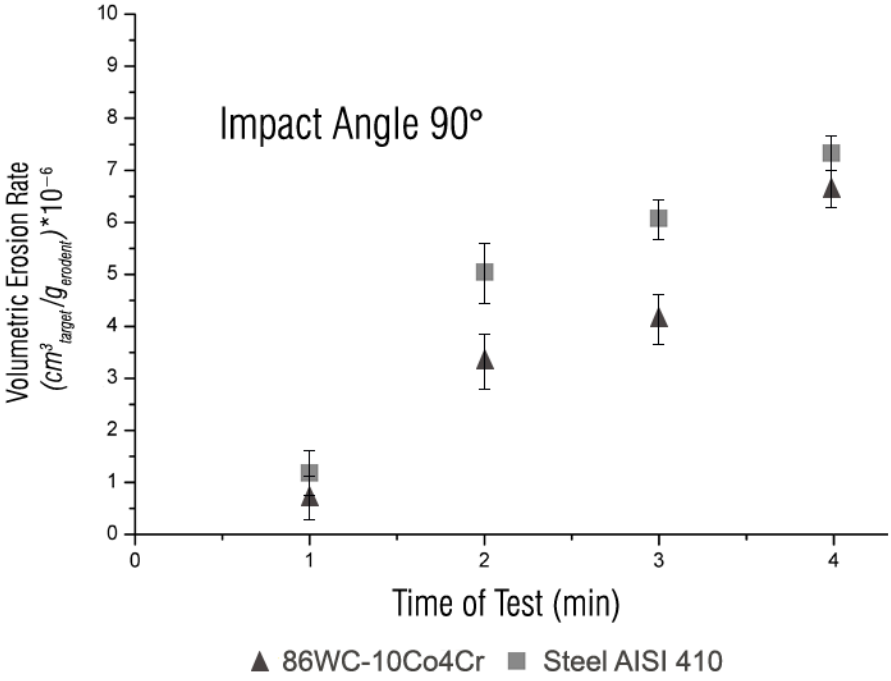

Figure 10. Variation of the accumulated volumetric erosion rate as a function of the impact angle of 90° for the martensitic stainless steel (AISI 410) and tungsten carbide (86WC-10Co-4Cr) coating.

Figure 11 shows, in detail, the eroded areas of the materials subjected to the jet slurry test for the impact angles of 30° and 90°. It is observed that the eroded region of the pieces (highlighted in red) for the 30° angle have an elongated shape and greater eroded area. The erosion of the specimens tested at 90° is more localized, and has a smaller area and a greater depth. The formation of the concentric ring, also known as "halo" erosion, can be observed, which is a mechanical characteristic of the damage due to the development of craters that appear as macro pits on the surface for this angle [51–53]. The roughness of these eroded regions is displayed in Table 5.

Table 5. Average roughness of coating and substrate before and after jet slurry erosion.

Roughness Ra (μm)					
Material/Coating	**Before Erosion**	**Standard Deviation**	**Angle (°)**	**After Erosion**	**Standard Deviation**
*86*WC-10Co4Cr	0.08	0.02	30	1.60	0.11
			90	1.91	0.13
Steel AISI 410	0.07	0.03	30	2.97	0.47
			90	2.56	0.11

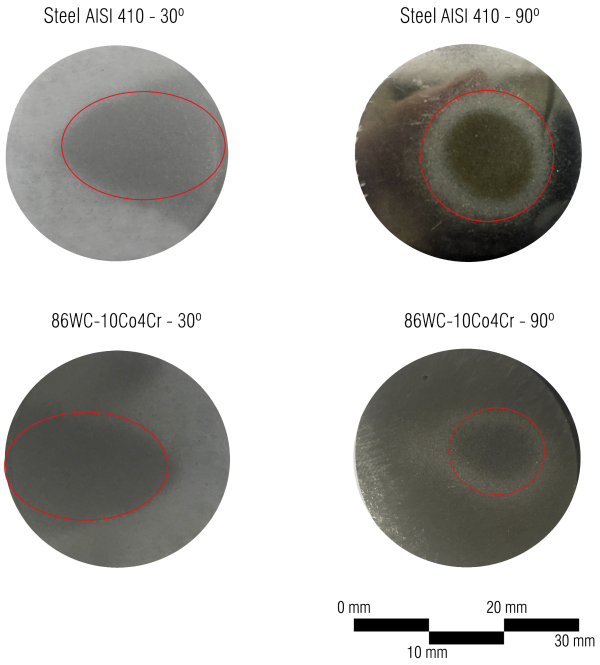

Figure 11. Eroded regions of the materials submitted to the jet slurry test obtained by Image J software (LM, 50×).

Table 6 shows the eroded areas as a function of the impact angle. It is observed that the area is greater for the impact angle of 30°. Compared to the substrate, the coating presented smaller eroded areas for the two impact angles studied.

Table 6. Eroded area as a function of the impact angle for both martensitic stainless steel (AISI 410) and tungsten carbide (86WC-10Co-4Cr) coating.

Material/Coating	Impact Angle (°)	Eroded Area (mm^2)
Steel AISI 410	30	277.7
	90	147.1
86WC-10Co4Cr	30	201.2
	90	94.9

Figure 12 represents the entire surfaces of the specimens' upper cylindrical faces, and elliptical shapes were attained because the coupons were rotated in order for the 3D laser scan to be able to accurately capture the eroded depth. Table 7 shows the respective average erosion depths. As expected, given that 90° tests resulted in more localized worn areas, their depth is superior to those found in samples tested at 30°.

Islam et al. [43] conducted an erosion study in steel tubes, varying both impact angle and velocity, obtaining significantly deeper erosion areas for 90° than for 30°, supporting the results which were hereby found. Similarly, Vite-Torres et al. [53] investigated the performance of the AISI 420 stainless steel subjected to particle erosion tests using two different abrasives at the angles of incidence of 30°, 45°, 60°, and 90°. Their results also demonstrated that the samples evaluated at 90° presented a greater depth profile than those of 30° tested independently of the abrasive which was adopted.

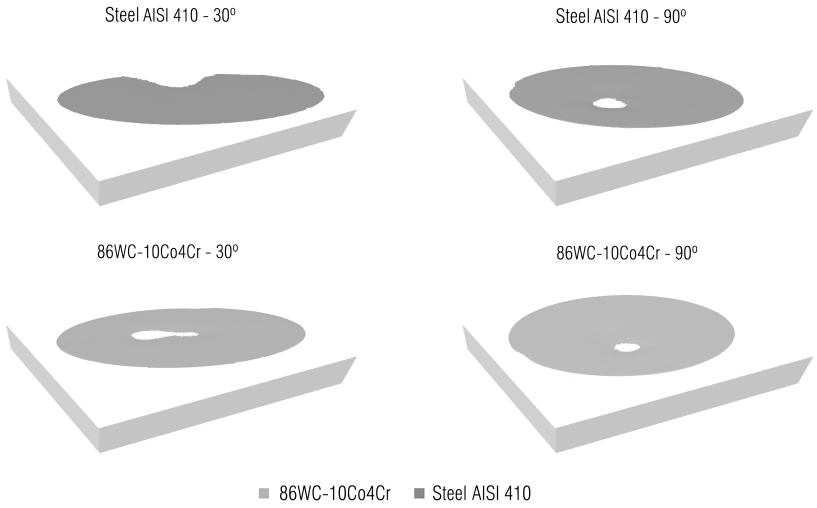

Figure 12. Three-dimensional scanning of the samples submitted to the jet slurry erosion test obtained the eroded depth by using the Geomagic Studio software (Version 2012.1.1, 3D Systems Inc, Rock Hill, SC, USA).

Table 7. Average depth of the eroded regions for substrate and coating.

Material/Coating	Impact Angle (°)	Average Depth (μm)	Standard Deviation (μm)
Steel AISI 410	30	93	±2.88
	90	102	±15.87
86WC-10Co4Cr	30	33	±5.77
	90	62	±3.21

4. Conclusions

In the present investigation, an experimental wear simulation equipment of jet slurry erosion was developed with conditions that allowed for the control of the significant test parameters, such as impact angle, impact velocity, erosive particle concentration in the suspension, and test temperature. The jet slurry erosion behaviors of martensitic stainless steel (AISI 410) and tungsten carbide (86WC-10Co-4Cr) coating were investigated, and from the results obtained in this experimental work, it is possible to infer the following conclusions:

1. The tungsten carbide coating showed higher resistance to jet slurry erosion compared to martensitic stainless steel, possibly due to the low porosity, the hardness of WC particles, and better properties of the CoCr binder material matrix. Thus, the application of such a coating can be considered as beneficial for the structural endurance of the substrate in applications where the part is subjected to similar erosive conditions.
2. The high concentration of WC-Co in the coating blend promotes greater hard-phase connectivity, leading to increased mechanical strength and jet slurry erosion resistance.
3. The martensitic stainless steel presented a higher rate of accumulated volumetric erosion in the impact angle of 30°, denoting ductile behavior. On the other hand, the accumulated volumetric erosion rate for tungsten carbide coating was higher at the impact angle of 90°, indicating a predominantly brittle failure mechanism.
4. For the impact angle of 30°, the tungsten carbide coating presented a cumulative volumetric erosion rate of approximately 50% less than martensitic stainless steel.

5. Patents

For the development of the research a jet slurry erosion tester was designed which is in the patent process by the INPI agency of the Brazilian government with Process Number BR 20 2018 074233 2.

Author Contributions: Conceptualization, C.P.B. and A.S.T.; Methodology, G.S., C.P.B. and A.S.T.; Software, G.S.; Validation, G.S. and F.V.d.C.; Formal Analysis, G.S. and A.S.T.; Investigation, G.S.; Data Curation, G.S. and F.V.d.C.; Writing-Original Draft Preparation, G.S. and F.V.d.C.; Writing-Review C.P.B., C.F. and F.V.d.C.; Supervision, C.P.B., C.F. and A.S.T.; Project Administration, G.S., C.P.B. and A.S.T.

Funding: This research was funded by the Coordination of Improvement of Higher Education Personnel of the Brazilian Ministry of Education (CAPES/MEC), grant numbers 88882.345871/2019-01 and 88882.345831/2019-01.

Acknowledgments: The authors express their gratitude to the following laboratories: Laboratory of Ceramic Materials (LACER), Laboratory of Physical Metallurgy (LAMEF), Laboratory of Design and Selection of Materials (LdSM) and the Laboratory of Conventional Machining (LUC) of the Engineering Institute of the Federal University of Rio Grande do Sul (UFRGS) for the investigation support and to the Research and Technology Center of Rijeza Metallurgy. G.S. and F.V.d.C. thank the Coordination of Improvement of Higher Education Personnel of the Brazilian Ministry of Education (CAPES/MEC) for the doctorate scholarship.

Conflicts of Interest: The authors declare no conflict of interest.

References

1. Popov, V.L. Adhesive wear: Generalized Rabinowicz'criteria. *Facta Univ. Ser. Mech. Eng.* **2018**, *16*, 29–39. [CrossRef]
2. López-Ortega, A.; Bayón, R.; Arana, J.L. Evaluation of Protective Coatings for High-Corrosivity Category Atmospheres in Offshore Applications. *Materials* **2019**, *12*, 1325. [CrossRef]
3. Mohrbacher, H. Martensitic automotive steel sheet-fundamentals and metallurgical optimization strategies. Advanced Materials Research. *Trans. Tech. Publ.* **2015**, *1063*, 130–142.
4. Klueh, R.; Nelson, A.T. Ferritic/martensitic steels for next-generation reactors. *J. Nucl. Mater.* **2007**, *371*, 37–52. [CrossRef]
5. Abe, F. Precipitate design for creep strengthening of 9% Cr tempered martensitic steel for ultra-supercritical power plants. *Sci. Technol. Adv. Mater.* **2008**, *9*, 013002. [CrossRef]
6. Krauss, G. *Steels: Processing, Structure, and Performance*; Asm International: Novelty, OH, USA, 2015.
7. Levy, A.V.; Yau, P. Erosion of steels in liquid slurries. *Wear* **1984**, *98*, 163–182. [CrossRef]
8. Kumar, R.; Kamaraj, M.; Seetharamu, S.; Pramod, T.; Sampathkumaran, P. Effect of Spray Particle Velocity on Cavitation Erosion Resistance Characteristics of HVOF and HVAF Processed 86WC-10Co4Cr Hydro Turbine Coatings. *J. Therm. Spray Technol.* **2016**, *25*, 1217–1230, doi:10.1007/s11666-016-0427-3. [CrossRef]
9. Bergmann, C.P.; Vicenzi, J. Protection against erosive wear using thermal sprayed cermet: A review. In *Protection against Erosive Wear Using Thermal Sprayed Cermet*; Springer: Berlin, Germany, 2011; pp. 1–77.
10. Cunha, M.A.; Guaglianoni, W.C.; Bezerra, B.F.A.; de Camargo, F.V.; Bergmann, C.P. Resistance to Abrasive and Erosive Wear of WCCo/NiCr HVOF Coatings: Comparative Evaluation of Commercial Nanostructured Spray Powders. *Tribol. Ind.* **2019**, in press.
11. Totemeier, T.C.; Wright, R.N.; Swank, W. FeAl and Mo-Si-B intermetallic coatings prepared by thermal spraying. *Intermetallics* **2004**, *12*, 1335–1344, doi:10.1016/j.intermet.2004.04.034. [CrossRef]
12. Ahledel, N.; Schulz, R.; Gariepy, M.; Hermawan, H.; Alamdari, H. Electrochemical Corrosion Behavior of Fe_3Al/TiC and Fe_3Al-Cr/TiC Coatings Prepared by HVOF in NaCl Solution. *Metals* **2019**, *9*, 437. [CrossRef]
13. Zhang, J.; Deng, C.; Song, J.; Deng, C.; Liu, M.; Dai, M. Electrochemical Corrosive Behaviors of Fe-Based Amorphous/Nanocrystalline Coating on Stainless Steel Prepared by HVOF-Sprayed. *Coatings* **2019**, *9*, 226. [CrossRef]
14. Liu, W.H.; Shieu, F.S.; Hsiao, W.T. Enhancement of wear and corrosion resistance of iron-based hard coatings deposited by high-velocity oxygen fuel (HVOF) thermal spraying. *Surf. Coat. Technol.* **2014**, *249*, 24–41. [CrossRef]
15. Hou, G.; An, Y.; Zhao, X.; Zhou, H.; Chen, J. Effect of alumina dispersion on oxidation behavior as well as friction and wear behavior of HVOF-sprayed CoCrAlYTaCSi coating at elevated temperature up to 1000 °C. *Acta Mater.* **2015**, *95*, 164–175. [CrossRef]
16. Nahvi, S.; Jafari, M. Microstructural and mechanical properties of advanced HVOF-sprayed WC-based cermet coatings. *Surf. Coat. Technol.* **2016**, *286*, 95–102. [CrossRef]
17. Hong, S.; Wu, Y.; Zhang, J.; Zheng, Y.; Zheng, Y.; Lin, J. Synergistic effect of ultrasonic cavitation erosion and corrosion of WC–CoCr and FeCrSiBMn coatings prepared by HVOF spraying. *Ultrason. Sonochem.* **2016**, *31*, 563–569. [CrossRef]

18. FEITAL Group. 2019. Available online: www.feital.com.br/produtos/ (accessed on 23 May 2019).
19. Oerlikon Metco Company. 2019. Available online: https://www.oerlikon.com/metco/en/products-services/coating-materials/coating-materials-thermal-spray/cermets/ (accessed on 23 May 2019).
20. International Organization for Standardization. *Particle Size Analysis—Laser Diffraction Methods*; ISO Standards Authority: Geneva, Switzerland, 2009.
21. ASTM International. *E2109-01 (2014) Standard Test Methods for Determining Area Percentage Porosity in Thermal Sprayed Coatings*; ASTM International: West Conshohocken, PA, USA, 2014.
22. ASTM International. *Standard Test Method for Knoop and Vickers Hardness of Materials*; ASTM International: West Conshohocken, PA, USA, 2011.
23. ASTM International. *ASTM G76-13 (2013) Standard Test Method for Conducting Erosion Tests by Solid Particle Impingement Using Gas Jets*; ASTM International: West Conshohocken, PA, USA, 2013.
24. Zu, J.; Hutchings, I.; Burstein, G. Design of a slurry erosion test rig. *Wear* **1990**, *140*, 331–344. [CrossRef]
25. Wentzel, E.; Allen, C. The erosion-corrosion resistance of tungsten-carbide hard metals. *Int. J. Refract. Met. Hard Mater.* **1997**, *15*, 81–87. [CrossRef]
26. Santa, J.; Baena, J.; Toro, A. Slurry erosion of thermal spray coatings and stainless steels for hydraulic machinery. *Wear* **2007**, *263*, 258–264. [CrossRef]
27. Santa, J.; Espitia, L.; Blanco, J.; Romo, S.; Toro, A. Slurry and cavitation erosion resistance of thermal spray coatings. *Wear* **2009**, *267*, 160–167. [CrossRef]
28. Hutchings, I. A model for the erosion of metals by spherical particles at normal incidence. *Wear* **1981**, *70*, 269–281. [CrossRef]
29. Finnie, I. Some reflections on the past and future of erosion. *Wear* **1995**, *186*, 1–10. [CrossRef]
30. Maiti, A.; Mukhopadhyay, N.; Raman, R. Improving the wear behavior of WC-CoCr-based HVOF coating by surface grinding. *J. Mater. Eng. Perform.* **2009**, *18*, 1060. [CrossRef]
31. Madsen, B.W. Measurement of erosion-corrosion synergism with a slurry wear test apparatus. *Wear* **1988**, *123*, 127–142. [CrossRef]
32. Murthy, J.; Rao, D.; Venkataraman, B. Effect of grinding on the erosion behaviour of a WC-Co-Cr coating deposited by HVOF and detonation gun spray processes. *Wear* **2001**, *249*, 592–600. [CrossRef]
33. Liu, X.; Zhang, B. Effects of grinding process on residual stresses in nanostructured ceramic coatings. *J. Mater. Sci.* **2002**, *37*, 3229–3239. [CrossRef]
34. File, P.D. *Joint Committee on Powder Diffraction Standards*; ASTM International: West Conshohocken, PA, USA, 1967; pp. 9–185.
35. Chivavibul, P.; Watanabe, M.; Kuroda, S.; Kawakita, J.; Komatsu, M.; Sato, K.; Kitamura, J. Effects of particle strength of feedstock powders on properties of warm-sprayed WC-Co coatings. *J. Therm. Spray Technol.* **2011**, *20*, 1098–1109. [CrossRef]
36. Guilemany, J.; De Paco, J.; Miguel, J.; Nutting, J. Characterization of the W2C phase formed during the high velocity oxygen fuel spraying of a WC + 12pct Co powder. *Metall. Mater. Trans. A* **1999**, *30*, 1913–1921. [CrossRef]
37. Thakur, L.; Arora, N.; Jayaganthan, R.; Sood, R. An investigation on erosion behavior of HVOF sprayed WC-CoCr coatings. *Appl. Surf. Sci.* **2011**, *258*, 1225–1234. [CrossRef]
38. Castro, G.; Arenas, F.; Rodriguez, M.; Scagni, A. Microestructura De materiales compuestos WC-Co/Ni-W-Cr recubiertos Por HVOF. *Rev. Latinoam. Metal. Mater.* **2001**, *21*, 50–55.
39. Castro, R.; Rocha, A.; Cavaler, L.; Kejelin, N.; Marques, F. Avaliação das características de superfície e do desgaste abrasivo de revestimentos aplicados em hastes de cilindros hidráulicos pelas técnicas de aspersão (HVOF) e eletrodeposição. Master's Thesis, Federal University of Rio Grande do Sul, Porto Alegre, Brazil, 2012.
40. Solution, T.S. Hydraulic Seals/Rod Seals. Available online: http://tk-ines.ru/upload/iblock/26e/26e36169a1738d5faa13585f921374e1.PDF (accessed on 23 May 2019).
41. Berger, L.M.; Saaro, S.; Naumann, T.; Wiener, M.; Weihnacht, V.; Thiele, S.; Suchánek, J. Microstructure and properties of HVOF-sprayed chromium alloyed WC-Co and WC–Ni coatings. *Surf. Coat. Technol.* **2008**, *202*, 4417–4421. [CrossRef]
42. Ahmed, R.; Ali, O.; Faisal, N.H.; Al-Anazi, N.; Al-Mutairi, S.; Toma, F.L.; Berger, L.M.; Potthoff, A.; Goosen, M. Sliding wear investigation of suspension sprayed WC-Co nanocomposite coatings. *Wear* **2015**, *322*, 133–150. [CrossRef]

43. Islam, M.A.; Farhat, Z.N. Effect of impact angle and velocity on erosion of API X42 pipeline steel under high abrasive feed rate. *Wear* **2014**, *311*, 180–190. [CrossRef]
44. Okonkwo, P.C.; Shakoor, R.A.; Zagho, M.M.; Mohamed, A.M.A. Erosion Behaviour of API X100 Pipeline Steel at Various Impact Angles and Particle Speeds. *Metals* **2016**, *6*, 232. [CrossRef]
45. Bayer, R.G. *Mechanical Wear Prediction and Prevention*; Marcel Dekker, Inc.: Monticello, NY, USA, 1994.
46. Papini, M.; Spelt, J. The plowing erosion of organic coatings by spherical particles. *Wear* **1998**, *222*, 38–48. [CrossRef]
47. O'Flynn, D.; Bingley, M.; Bradley, M.; Burnett, A. A model to predict the solid particle erosion rate of metals and its assessment using heat-treated steels. *Wear* **2001**, *248*, 162–177. [CrossRef]
48. Biswas, S.; Satapathy, A.; Patnaik, A. Erosion wear behavior of polymer composites: A review. *J. Reinf. Plast. Compos.* **2010**, *29*, 2898–2924. [CrossRef]
49. Barber, J.; Mellor, B.; Wood, R. The development of sub-surface damage during high energy solid particle erosion of a thermally sprayed WC-Co-Cr coating. *Wear* **2005**, *259*, 125–134. [CrossRef]
50. Javaheri, V.; Porter, D.; Kuokkala, V.T. Slurry erosion of steel—Review of tests, mechanisms and materials. *Wear* **2018**, *408*, 248–273. [CrossRef]
51. Wood, F.W. Erosion by solid-particle impacts: A testing update. *J. Test. Eval.* **1986**, *14*, 23–27.
52. De Souza, V.; Neville, A. Corrosion and erosion damage mechanisms during erosion–corrosion of WC-Co-Cr cermet coatings. *Wear* **2003**, *255*, 146–156. [CrossRef]
53. Vite-Torres, M.; Laguna-Camacho, J.; Baldenebro-Castillo, R.; Gallardo-Hernandez, E.A.; Vera-Cárdenas, E.; Vite-Torres, J. Study of solid particle erosion on AISI 420 stainless steel using angular silicon carbide and steel round grit particles. *Wear* **2013**, *301*, 383–389. [CrossRef]